


Cite this: *RSC Adv.*, 2021, 11, 28940

The kinetics and mechanism of H₂O₂ decomposition at the U₃O₈ surface in bicarbonate solution

John McGrady,^a Yuta Kumagai,^a Masayuki Watanabe,^a Akira Kirishima,^b Daisuke Akiyama,^b Akira Kitamura^c and Shingo Kimuro^c

In the event of nuclear waste canister failure in a deep geological repository, groundwater interaction with spent fuel will lead to dissolution of uranium (U) into the environment. The rate of U dissolution is affected by bicarbonate (HCO₃[−]) concentrations in the groundwater, as well as H₂O₂ produced by water radiolysis. To understand the dissolution of U₃O₈ by H₂O₂ in bicarbonate solution (0.1–50 mM), dissolved U concentrations were measured upon H₂O₂ addition (300 μM) to U₃O₈/bicarbonate mixtures. As the H₂O₂ decomposition mechanism is integral to the dissolution of U₃O₈, the kinetics and mechanism of H₂O₂ decomposition at the U₃O₈ surface was investigated. The dissolution of U₃O₈ increased with bicarbonate concentration which was attributed to a change in the H₂O₂ decomposition mechanism from catalytic at low bicarbonate (≤5 mM HCO₃[−]) to oxidative at high bicarbonate (≥10 mM HCO₃[−]). Catalytic decomposition of H₂O₂ at low bicarbonate was attributed to the formation of an oxidised surface layer. Second-order rate constants for the catalytic and oxidative decomposition of H₂O₂ at the U₃O₈ surface were 4.24 × 10^{−8} m s^{−1} and 7.66 × 10^{−9} m s^{−1} respectively. A pathway to explain both the observed U₃O₈ dissolution behaviour and H₂O₂ decomposition as a function of bicarbonate concentration was proposed.

Received 21st July 2021
Accepted 13th August 2021

DOI: 10.1039/d1ra05580a

rsc.li/rsc-advances

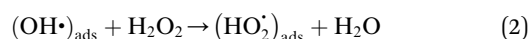
Introduction

The current strategy for the disposal of spent nuclear fuel is in a deep geological repository according to the majority of the international community. The repositories provide a long-term storage solution, yet the release of radioactive species from spent nuclear fuel into the environment from the repository is projected to occur in the future upon failure of the repository barriers. Therefore, it is necessary to develop safety models for the repositories to predict their performance when failure occurs and nuclear material is exposed to the local environment. The main pathway for radionuclide release is predicted to be caused by the ingress of groundwater into the repository and interaction of the groundwater with the surface of the spent fuel. Understanding the reaction mechanisms between groundwater and spent fuel is integral to the development of safety models. Such interactions between the groundwater and spent fuel will lead to dissolution of the UO₂ matrix which constitutes the majority of the spent fuel.¹ The solubility of U in

groundwater is governed by the form of U (U^(IV), U^(V) and U^(VI)), with the hexavalent U^(VI) form being more soluble than U^(IV) and U^(V).^{2–4} Therefore, the presence of U^(VI) facilitates U dissolution into the groundwater upon canister failure.

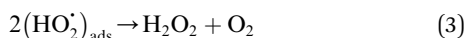
Under the reducing, anoxic conditions typically found in groundwater at repository depths, the solubility of U^(IV) is very low,^{5–7} and so significant dissolution of the UO₂ spent fuel may not be expected. However, radiation from the spent fuel will cause radiolysis of fuel adjacent water leading to the formation of a complex water chemistry involving radical, ionic and molecular species in the form of both reductants (e_{aq}[−], H[•], H₂) and oxidants (OH[•], H₂O₂).⁸ This will significantly affect the local redox chemistry of the water and the oxidation state of U.

Of the oxidants generated by radiolysis, it has been shown that H₂O₂ is the dominant species in regards to U dissolution under deep geological repository conditions.^{9,10} The interaction of H₂O₂ with the UO₂ surface has been thoroughly studied due to its importance for U dissolution, and it has been proposed that there are two competing pathways, both of which involve the decomposition of H₂O₂ at the UO₂ surface.^{11,12} The first involves catalytic H₂O₂ decomposition forming H₂O₂ and O₂ where the UO₂ surface acts as a catalyst (ads = adsorbed):

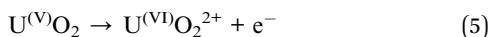
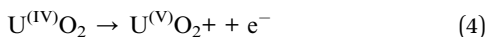

^aNuclear Science and Engineering Center, Japan Atomic Energy Agency (JAEA), Tokai, Ibaraki, 319-1195, Japan. E-mail: mcgrady.john@jaea.go.jp; kumagai.yuta@jaea.go.jp

^bInstitute of Multidisciplinary Research for Advanced Materials, Tohoku University, 1-1 Katahira, 2-chome, Aoba-ku, Sendai 980-8577, Japan

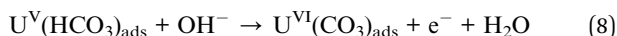
^cRadionuclide Migration Research Group, Japanese Atomic Energy Agency (JAEA), Tokai, Ibaraki, 319-1195, Japan

In this case, the H_2O_2 decomposition does not directly cause U dissolution. The second is an oxidative decomposition reaction where H_2O_2 oxidises $\text{U}^{(\text{IV})}$ to $\text{U}^{(\text{V})}$ (eqn (4)) and $\text{U}^{(\text{V})}$ to $\text{U}^{(\text{VI})}$ (eqn (5)) while itself being reduced to OH^- (eqn (6)) in a redox couple.



Typically, groundwater also contains bicarbonate (HCO_3^-) which has been shown to enhance the dissolution of U due to favourable complexation with $\text{U}^{(\text{VI})}$ and stabilisation of the dissolution products:^{13–16}



Therefore, the concentration of bicarbonate is believed to have a significant effect on U dissolution and the rate of H_2O_2 decomposition at the UO_2 surface.

Due to the importance of developing models to predict U dissolution into groundwater, various studies have been undertaken with UO_2 in simulated groundwater. A recent study by Kumagai *et al.*¹⁷ has shown that increasing the oxygen content from UO_2 to $\text{UO}_{2.3}$ increased U dissolution and reduced the rate of H_2O_2 decomposition at the oxide surface. As the dissolution of U is governed by the redox behaviour of the U atoms, it follows that the ratio of $\text{U}^{(\text{IV})}$, $\text{U}^{(\text{V})}$ and $\text{U}^{(\text{VI})}$ will have a significant impact on both U dissolution as well as the H_2O_2 decomposition pathway. Therefore, the form of uranium oxide that exists on the spent fuel oxide will have a large effect on the dissolution of U into the environment. Due to the radiolysis of spent fuel surface adjacent groundwater and the elevated temperatures from spent fuel decay, the formation of highly oxidised forms of U is expected *i.e.*, where $x > 0.3$ for UO_{2+x} . However, there is still a lack of knowledge regarding the impact of higher oxidised forms of U on the mechanism of U dissolution and H_2O_2 decomposition.

To investigate this, we adopted U_3O_8 as an extreme case, which corresponds to $\text{UO}_{2.66}$ containing two $\text{U}^{(\text{V})}$ atoms and one $\text{U}^{(\text{VI})}$ atom.^{18–20} U_3O_8 has been observed on used nuclear fuel both in wet²¹ and air^{22,23} environments, and can be used as a highly oxidised form of uranium oxide for an examination of the effects of U valence on U dissolution. As the complexation of bicarbonate with $\text{U}^{(\text{VI})}$ is thought to drive U dissolution by favourable complexation, the effect of U oxidation state on the dissolution of U in bicarbonate solution can be investigated by using U_3O_8 . The H_2O_2 decomposition mechanism is dependent

on U oxidation and so can also be investigated using U_3O_8 for comparison with UO_2 . The concentration of bicarbonate in groundwater is dependent on the location of the deep geological repository, and can range from $\sim 10^{-4}$ M (Tono, Japan),²⁴ to $\sim 10^{-3}$ M (Daejeon, South Korea),^{25,26} to $\sim 10^{-2}$ M (Forsmark, Sweden)²⁷ and so it is necessary to understand U dissolution and H_2O_2 decomposition at uranium oxide surfaces over a range of bicarbonate concentrations.

Therefore, in this work, U dissolution from U_3O_8 suspensions with H_2O_2 as a function of sodium bicarbonate (NaHCO_3) has been investigated, and the mechanism of H_2O_2 decomposition at the U_3O_8 surface has been elucidated.

Experimental

Materials

Two samples of U_3O_8 powder were used in this study to investigate the reproducibility of the U dissolution tests. The first U_3O_8 powder (sample 1) was prepared by heating UO_2 powder to 750 °C for 3 hours under a continuous flow of air. The second (sample 2) was prepared by dissolving U metal in 13 M HNO_3 (Fujifilm Wako Pure Chemical, 60%) to form $\text{UO}_2(\text{NO}_3)_2 \cdot (\text{H}_2\text{O})_n$, which was then heated under identical conditions to give a 96% yield of U_3O_8 . The formation of U_3O_8 was confirmed by XRD and the data was refined using the Rietveld method.²⁸ The average crystallite size was measured using the Scherrer equation:²⁹

$$d = \frac{0.9\lambda}{b \cos \theta} \quad (10)$$

where d is the mean crystallite size, λ is the X-ray wavelength (1.5406 Å), b is the full width at half maximum value, and θ is the diffraction peak position. The crystallite sizes were calculated as 47 and 46 nm for sample 1 and 2 respectively. The orthorhombic lattice constants were also calculated from the diffractograms using Bragg's law³⁰ for orthorhombic structures ($1/d_{hkl}^2 = h^2/a^2 + k^2/b^2 + l^2/c^2$) giving values of $a = 6.72$, $b = 11.96$ and $c = 4.15$ Å for sample 1 and $a = 6.71$, $b = 11.95$ and $c = 4.14$ Å for sample 2. The lattice constants were consistent with those for U_3O_8 ($a = 6.72$, $b = 11.96$ and $c = 4.15$ Å).³¹ This indicated that the structure of each U_3O_8 sample prepared *via* different methods was almost identical. Sample 1 was used for determination of the pseudo-first order rate constants for H_2O_2 decomposition to investigate the mechanism of decomposition. Sample 2 was used for determination of the second order rate constants for H_2O_2 decomposition at the U_3O_8 surface for comparison with UO_2 . This assignment was solely due to the amount of sample required to conduct each set of experiments – there was an insufficient amount of sample 1 for the second order experiments. The reproducibility of the dissolution tests with different U_3O_8 samples could then be analysed by comparison of H_2O_2 decomposition rates on each sample. The specific surface area of the powders was measured for calculation of the second order rate constants. Specific surface areas were measured by the Brunauer–Emmett–Teller method³² of adsorption/desorption using Kr gas with a Micromeritics Tristar II instrument. This method involves the adsorption of a monolayer of gas onto the surface of the powder at cryogenic



temperatures, and the volume of adsorbed gas provides surface area information. Values of $1.20 \text{ m}^2 \text{ g}^{-1}$ and $2.52 \pm 0.2 \text{ m}^2 \text{ g}^{-1}$ for sample 1 and sample 2 were obtained respectively. After the immersion tests, the U_3O_8 powder was dried under vacuum and analysed by Raman spectroscopy to investigate alterations to the U_3O_8 surface.

Dissolution experiments

The effect of NaHCO_3 (Alfa Aesar) on the dissolution of U_3O_8 powder by reaction with H_2O_2 (Fujifilm Wako Pure Chemical, 30%) was investigated by monitoring the U and H_2O_2 concentration as a function of reaction time. A suspension of U_3O_8 was prepared at concentrations of NaHCO_3 between 0.1–50 mM (pH 8.2–9.7), and the suspensions were purged with Ar for approximately 18 hours to ensure removal of O_2 to imitate the anoxic conditions of groundwater. Into the suspension, H_2O_2 was added to initiate the reaction. The concentration of H_2O_2 added was 300 μM which has been shown to be optimal to study oxidative dissolution on UO_2 .¹⁷ Ar purging was continued throughout the experiment. Experiments were conducted under atmospheric pressure at a temperature of 25 °C which was maintained with a coolant system. Samples of the suspension were taken at intervals over the course of the reaction. The samples were immediately filtered through a 0.45 μm filter to stop the reaction, and then analysed for H_2O_2 and U. For determination of the pseudo-first order rate constants, 50 mg of U_3O_8 (sample 1) was added to 50 ml bicarbonate solution, whilst for the second-order rate constant measurements, 50, 100, 150 and 200 mg of U_3O_8 (sample 2) were added to 70 ml bicarbonate solution. Error in the experimental methodology was estimated as <5% by conducting a set of dissolution experiments in triplicate and taking the standard deviation of the H_2O_2 pseudo-first order decay constants.

Analytical techniques

The concentration of U was measured by ICP-OES using a PerkinElmer Avio-200 spectrometer. Calibration was conducted using U standards and measurements were done in triplicate. The standard deviations of the measurements were typically

<1% of the measured values. The concentration of H_2O_2 was measured by the Ghormley triiodide method where the iodide ion (I^-) reacts with H_2O_2 and is converted to triiodide (I_3^-) using ammonium heptamolybdate ($(\text{NH}_4)_6\text{Mo}_7\text{O}_{24}$) and an acidic buffer ($\text{KHC}_8\text{H}_4\text{O}_4$).^{33,34} The concentration of H_2O_2 was then determined from the absorbance spectra of I_3^- at 350 nm using a Shimadzu UV-3600 Plus UV-Vis-NIR spectrophotometer. Raman analysis of the oxide surface was conducted with a JASCO NRS-4500 Raman spectrometer. A 532 nm laser was introduced through a 20 \times objective lens, and 3 spectra of 10 seconds each were recorded and averaged for each sample.

Results and discussion

U dissolution

The dissolution of U upon addition of H_2O_2 to U_3O_8 suspensions as a function of NaHCO_3 was investigated by measuring dissolved U concentrations over the reaction time. Fig. 1 shows the dissolved uranium (U) minus the dissolved U concentration prior to H_2O_2 addition (U_0). The dissolution of U changed over the experimental time and showed a clear effect of bicarbonate on the dissolution of U_3O_8 . At $0.1 < [\text{NaHCO}_3] < 5 \text{ mM}$, the dissolution was low. At $> 5 \text{ mM}$ the extent of dissolution significantly increased with bicarbonate. This is due to a change in the H_2O_2 decomposition mechanism as discussed later. The magnitude of U dissolution decreased with increasing bicarbonate concentration (*i.e.*, from 5 to 10 mM bicarbonate the increase in U dissolution was $\sim 0.3 \text{ mM}$, and from 20 to 50 mM was $\sim 0.1 \text{ mM}$) indicating a complex relationship.

At $t = 1 \text{ min}$, the value of $[\text{U} - U_0]$ became negative at certain bicarbonate concentrations, and so the measured values of $[\text{U} - U_0]_{t=1\text{min}}$ were plotted as a function of bicarbonate concentration (Fig. 2). A decrease in the concentration of dissolved U can be seen in 5, 10 and 20 mM NaHCO_3 solution, suggesting deposition from solution of U onto the U_3O_8 surface after the initial addition of H_2O_2 as highlighted by the second y-axis. As the extent of deposition increased with bicarbonate, it can be predicted that the deposits are uranium carbonates. Under the

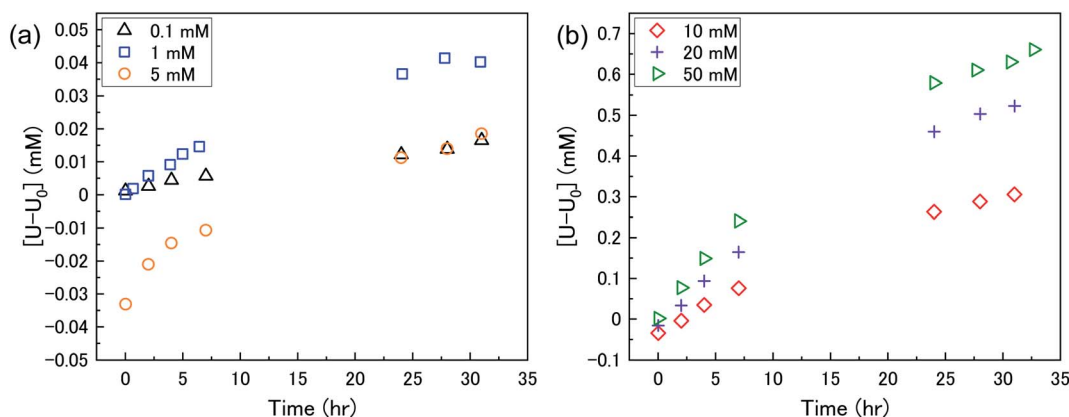


Fig. 1 The dissolution of U as a function of time in a 50 mg suspension of U_3O_8 (sample 1) in (a) 0.1, 1 and 5 mM bicarbonate and (b) 10, 20 and 50 mM bicarbonate solution after addition of 300 μM H_2O_2 .



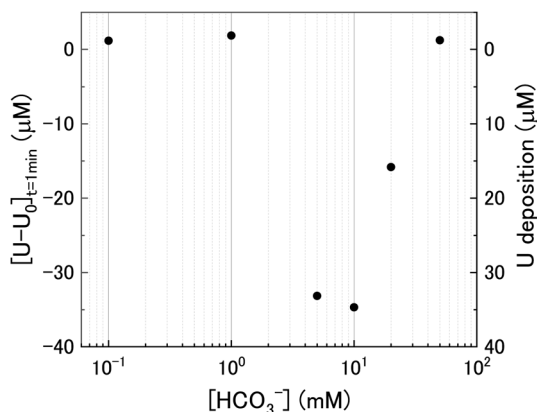


Fig. 2 The initial change in U concentration one minute after H_2O_2 addition to the U_3O_8 suspension as a function of bicarbonate concentration.

experimental conditions, the stable form of U in solution is $\text{UO}_2(\text{CO}_3)_3^{4-}$ and so the deposits may be $\text{UO}_2(\text{CO}_3)_3$. Another possibility is the formation of uranyl peroxide ($\text{UO}_2(\text{O}_2)_2$), where the increase in deposition with bicarbonate is due to an increase in dissolved U with bicarbonate and, therefore, an increase in uranyl peroxide.

Kinetics of H_2O_2 decomposition

The dissolution of U from U_3O_8 was induced by the addition of H_2O_2 to the bicarbonate solution. Therefore, to understand the observed U dissolution behaviour from U_3O_8 , the kinetics and mechanism of H_2O_2 decomposition at the U_3O_8 surface was studied. The kinetics of the reaction between H_2O_2 and U_3O_8 as a function of NaHCO_3 were investigated by measuring the concentration of H_2O_2 over the reaction time. Fig. 3 shows the concentration of H_2O_2 after adding 300 μM to a 50 mg suspension of U_3O_8 at different bicarbonate concentrations as a function of time. The H_2O_2 concentration decreased quickly at low bicarbonate concentration (0.1 mM), but the decomposition slowed down as the bicarbonate concentration increased to

5 mM. Further increases in the bicarbonate concentration up to 50 mM caused the rate of H_2O_2 decomposition to gradually increase again, until the H_2O_2 concentration profile in 50 mM bicarbonate was similar to that in 0.1 mM bicarbonate. The results in Fig. 3 clearly show an effect of bicarbonate on H_2O_2 decomposition on U_3O_8 .

To investigate the mechanism of H_2O_2 decomposition at the U_3O_8 surface, the kinetics of decomposition was investigated. Previous studies on H_2O_2 decomposition at the surface of uranium oxides have shown that the reaction follows first order kinetics with respect to H_2O_2 . As the U_3O_8 surface is in excess relative to H_2O_2 , the reaction can be modelled as a pseudo-first order reaction. Therefore, the rate of H_2O_2 decomposition can be explained by,

$$\frac{-d[\text{H}_2\text{O}_2]}{dt} = k_1[\text{H}_2\text{O}_2] \quad (11)$$

and the kinetics of H_2O_2 decomposition can be investigated by plotting the $\ln[\text{H}_2\text{O}_2]$ vs. time, where the gradient of the resulting straight-line plot gives the pseudo-first order rate constant, k , for the reaction (Fig. 4). The plots exhibited non-linear behaviour after the initial addition of H_2O_2 to the U_3O_8 /bicarbonate mixtures indicating an initial reaction of H_2O_2 with the U_3O_8 surface. This initial fast decomposition of H_2O_2 is attributed to the formation of a surface layer and is further discussed later.

The calculated values of k from the linear region (from $t = 2$ hours to the experiment end) are plotted against bicarbonate concentration in Fig. 5 and the value of k was found to be in the range between 0.4 to $1.6 \times 10^{-5} \text{ s}^{-1}$. The decrease in the pseudo-first order rate constant coincided with U deposition from solution indicating that the secondary phases that deposit on the surface of the U_3O_8 may block the approach of H_2O_2 to the surface. As the plots in Fig. 4 show linear behaviour, this suggests that these deposits are stable over the experimental timescale.

U dissolution with H_2O_2 decomposition

The mechanism of U dissolution *via* H_2O_2 decomposition can be investigated by analysing the extent of U dissolution as

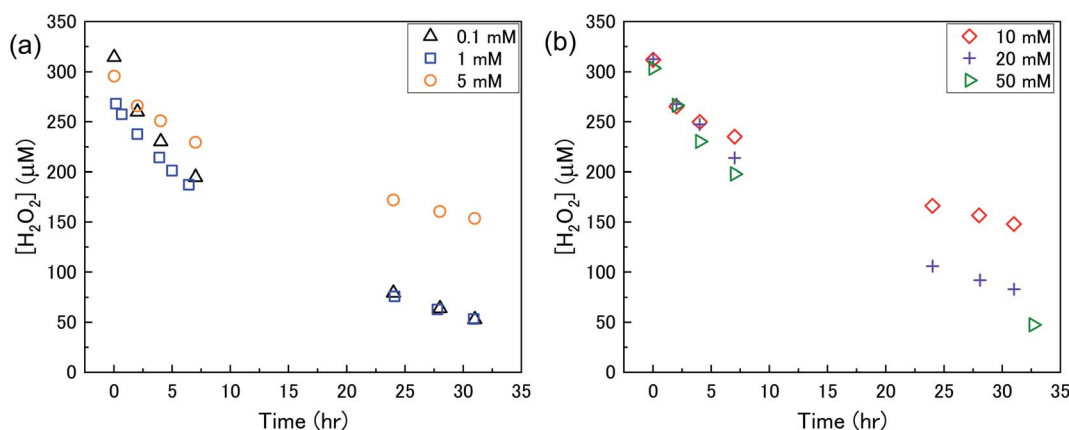


Fig. 3 The concentration of H_2O_2 as a function of time in a 50 mg suspension of U_3O_8 (sample 1) in (a) 0.1, 1 and 5 mM bicarbonate and (b) 10, 20 and 50 mM bicarbonate solution after addition of 300 μM H_2O_2 .



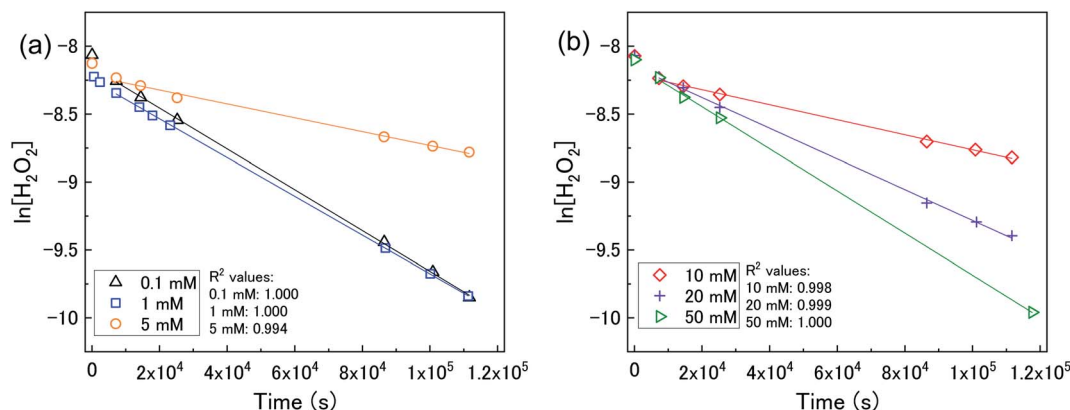


Fig. 4 (a) A plot of $\ln[\text{H}_2\text{O}_2]$ vs. time as a function of bicarbonate concentration with 50 mg U_3O_8 (sample 1) in (a) 0.1, 1 and 5 mM bicarbonate and (b) 10, 20 and 50 mM bicarbonate solution showing pseudo-first order behaviour.

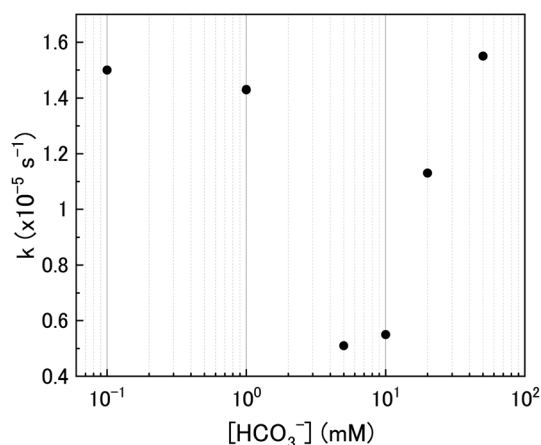


Fig. 5 The pseudo-first order rate constants for H_2O_2 decomposition.

a function of H_2O_2 decomposition. To illustrate this, Fig. 6 shows a plot of the amount of dissolved U against the amount of consumed H_2O_2 for each bicarbonate concentration. The U dissolution per H_2O_2 decomposition shows linear behaviour. If

we consider the oxidative pathway for H_2O_2 decomposition at the U_3O_8 surface, $\text{U}^{(\text{V})}$ is oxidised to $\text{U}^{(\text{VI})}$ leading to decomposition of the U_3O_8 unit since the net charge in the lattice is no longer neutral. Therefore, each H_2O_2 decomposition event *via* oxidative decomposition will lead to a U_3O_8 dissolution event ($\text{U}_3\text{O}_8 + \text{H}_2\text{O}_2 \rightarrow 3\text{UO}_2^{2+}(\text{aq})$), and a gradient of 3 may be expected from the plots in Fig. 6. If we consider only catalytic decomposition of H_2O_2 , no U dissolution would occur giving an ideal gradient of 0. Therefore, the measured gradients provide a ratio of oxidative to catalytic H_2O_2 decomposition at each bicarbonate concentration, assuming these pathways are the only pathways for H_2O_2 decomposition (*i.e.* for 50 mM bicarbonate the ratio of oxidative dissolution is $\frac{2.71}{3}$ and catalytic decomposition is $\frac{0.29}{3}$). The dissolution of U from U_3O_8 in

10 mM bicarbonate gave a gradient of 2.68. By comparison with the gradients measured from the dissolution of U from UO_2 (~ 0.4) and $\text{UO}_{2.3}$ (~ 1) with H_2O_2 addition in 10 mM bicarbonate,¹⁷ this shows that the oxidative dissolution of U increases with increased oxidation state of the uranium oxide. As the complexation of $\text{U}^{(\text{VI})}$ with bicarbonate drives the

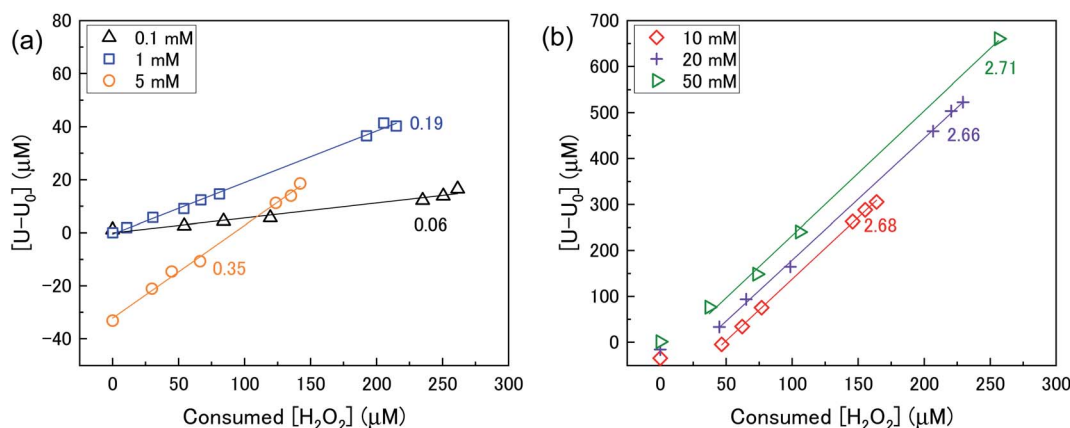


Fig. 6 U dissolution from a 50 mg U_3O_8 (sample 1) suspension as a function of consumed H_2O_2 in (a) 0.1, 1 and 5 mM bicarbonate and (b) 10, 20 and 50 mM bicarbonate solution.



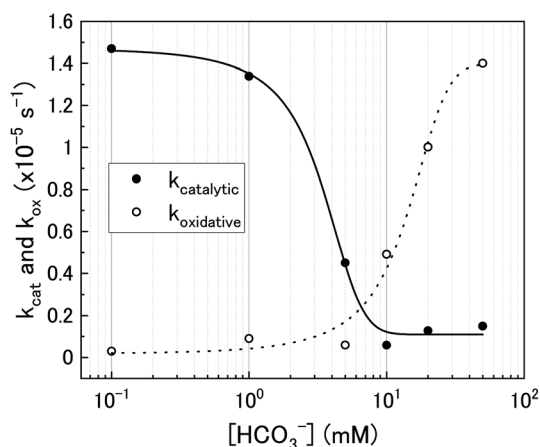


Fig. 7 The catalytic (k_{cat}) and oxidative (k_{ox}) pseudo-first order rate constants for H_2O_2 decomposition on U_3O_8 as a function of bicarbonate concentration.

dissolution of U from the surface, it follows that the two-step oxidation of $\text{U}^{(\text{IV})} \rightarrow \text{U}^{(\text{V})} \rightarrow \text{U}^{(\text{VI})}$ for UO_2 would result in less dissolution of U than the one-step oxidation for $\text{U}^{(\text{V})} \rightarrow \text{U}^{(\text{VI})}$ in U_3O_8 , and for intermediate UO_{2+x} stoichiometries the dissolution rate would increase with increasing values of x . Another point of consideration regarding U dissolution is the crystal structure of UO_2 (cubic fluorite) and U_3O_8 (orthorhombic). As the crystal structures are different, the number of surface sites for H_2O_2 decomposition will impact U dissolution. The surface site densities for UO_2 and U_3O_8 have been reported as between 126 (ref. 35) to 165 (ref. 36) sites per nm^2 for UO_2 and 48 (ref. 36) sites per nm^2 for U_3O_8 . As the surface sites are ~ 3 times lower for U_3O_8 , the observed increase in U dissolution from U_3O_8 relative to UO_2 is more pronounced than the measured dissolved U concentrations suggest.

Using the ratios taken from the gradients, the contributions of catalytic (k_{cat}) and oxidative (k_{ox}) decomposition to the measured pseudo-first order rate constant can be found and are plotted in Fig. 7 as a function of bicarbonate.

At low bicarbonate concentrations, the main pathway for H_2O_2 decomposition is the catalytic decomposition mechanism as there is little U dissolution associated with H_2O_2 decomposition. As k_{ox} is low, this indicates that the U_3O_8 is protected from H_2O_2 by a surface layer. It is postulated that upon addition of H_2O_2 to the bicarbonate solution, oxidative dissolution proceeds on the bare U_3O_8 surface (Fig. 8). As this involves the oxidation of $\text{U}^{(\text{V})}$ to $\text{U}^{(\text{VI})}$, it is likely that $\text{U}^{(\text{VI})}$ forms a surface layer on the U_3O_8 which protects against further oxidative

Proposed U_3O_8 surface layer formation upon H_2O_2 addition

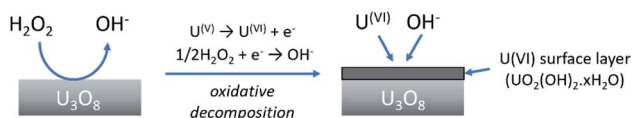


Fig. 8 The formation of a protective surface layer on the surface of U_3O_8 due to oxidative decomposition of H_2O_2 .

dissolution as $\text{U}^{(\text{VI})}$ is already fully oxidised, and due to the low concentration of bicarbonate the surface layer is stable.

The composition of the surface layer is thought to be in the hydroxide form $(\text{UO}_2(\text{OH})_2 \cdot x\text{H}_2\text{O})$ due to the formation of hydroxide from the oxidative decomposition of H_2O_2 . Raman analysis of the U_3O_8 surface after removal from solution and vacuum drying showed spectra representative of U_3O_8 only (Fig. 9). Peaks relating to U_3O_8 were observed including the U–O A_{1g} stretching modes at 335 and 410 cm^{-1} , and the U–O E_g stretching mode at 475 cm^{-1} .³⁷ As U_3O_8 was the only phase observed, any surface layer that formed had been removed prior to Raman analysis. If the surface layer is in the hydroxide form, it is expected to decompose upon drying which would explain the observed results. Further studies are required to elucidate the composition of the surface.

As the bicarbonate concentration increases from 0.1 to 5 mM, the rate of catalytic H_2O_2 decomposition decreases. This is caused by an increase in deposition from solution as seen in Fig. 2. As the pseudo-first order rate constant decreases up to 5 mM, it can be said that the deposits do not catalyse H_2O_2 decomposition to the extent that U_3O_8 does.

Increasing the bicarbonate concentration > 5 mM changes the main H_2O_2 decomposition mechanism pathway from catalytic to oxidative. At NaHCO_3 concentrations of 10 mM and above, at least 90% of the H_2O_2 decomposed *via* oxidation of $\text{U}^{(\text{V})}$ to $\text{U}^{(\text{VI})}$. This is due to increased dissolution of the $\text{U}^{(\text{VI})}$ surface layer and exposure of the U_3O_8 surface beneath leading an increase in k_{ox} . As the value of k increases with bicarbonate, this suggests that the dissolution step is rate determining rather than the redox reaction. Therefore, dissolution experiments in solutions of higher bicarbonate concentrations are required to elucidate the true value of k for oxidative dissolution in this system. Interestingly, a study by Nilsson *et al.* on UO_2 dissolution in 10 mM NaHCO_3 with H_2O_2 addition using pellets

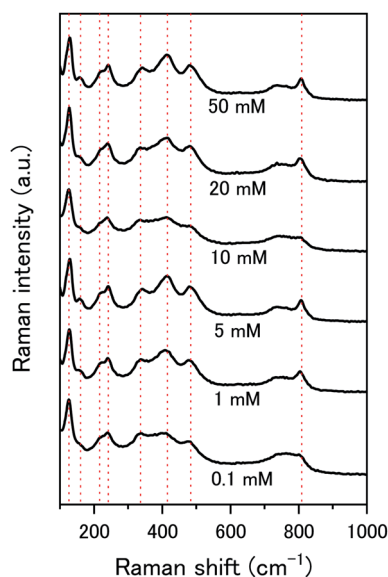


Fig. 9 Raman spectra of U_3O_8 (sample 1) after the dissolution tests for different concentrations of NaHCO_3 .



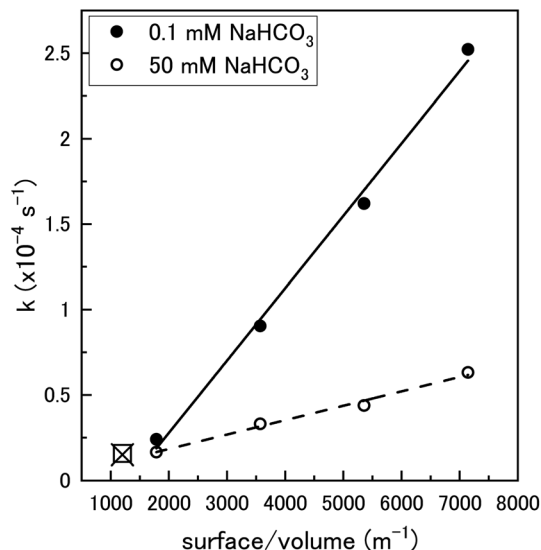


Fig. 10 The pseudo-first order rate constant, k , plotted against the U_3O_8 (sample 2) surface area to solution volume ratio (m^{-1}) for 0.1 mM and 50 mM HCO_3^- solutions (70 ml solution). The data for 0.1 mM (\square) and 50 mM (\times) calculated using U_3O_8 sample 1 shown in Fig. 5 is included to show reproducibility (50 mg U_3O_8 in 50 ml solution).

showed that $\sim 14\%$ of H_2O_2 decomposition events occurred *via* oxidative dissolution while the value was even lower ($\sim 2\%$) on SIMFUEL.³⁸ This suggests that k_{cat} is high in the case of the pellets indicating that the surface oxide that forms on the pellets is more protective than on the powders. The large discrepancy between the H_2O_2 decomposition behaviour between UO_2 pellets and U_3O_8 powder (and UO_2 powder) is a point that requires investigation.

To clarify the dependence of the catalytic and oxidative mechanisms on U_3O_8 , the second order rate constants for H_2O_2 decomposition were obtained for 0.1 mM and 50 mM solutions with U_3O_8 (sample 2). The second order rate equation,

$$-\frac{d[\text{H}_2\text{O}_2]}{dt} = k_2 \left(\frac{SA_{\text{U}_3\text{O}_8}}{V} \right) [\text{H}_2\text{O}_2] \quad (12)$$

can be used to obtain the second order rate constant by plotting the pseudo-first order rate constant against the U_3O_8 surface

area to total solution volume ratio (Fig. 10). The second order rate constant in 0.1 mM bicarbonate was $4.24 \times 10^{-8} \text{ m s}^{-1}$. At this concentration, the decomposition was shown to be almost completely catalytic, and so this can be attributed to the catalytic decomposition reaction pathway shown in eqn (1)–(3). At 50 mM, the value of the measured second order rate constant was $8.44 \times 10^{-9} \text{ m s}^{-1}$, and as the ratio of oxidative decomposition was $\sim 90\%$, we can estimate the oxidative decomposition rate constant to be $7.60 \times 10^{-9} \text{ m s}^{-1}$ for the pathway shown in eqn (5) and (6). These values are within the range described in the literature for catalytic decomposition (3.6×10^{-8} to $5 \times 10^{-11} \text{ m s}^{-1}$) and oxidative decomposition (1.4×10^{-7} to $2.0 \times 10^{-10} \text{ m s}^{-1}$) of H_2O_2 at the UO_2 surface.³⁹ The pseudo-first order rate constant measurement for 0.1 mM and 50 mM bicarbonate solutions using U_3O_8 sample 1 (shown in Fig. 5) are included in Fig. 10 showing the reproducibility of the data using different U_3O_8 powders.

Proposed pathway for U_3O_8 dissolution by H_2O_2 in NaHCO_3 solution

From the experimental results, a proposed pathway to explain the observed behaviour of U_3O_8 in bicarbonate solution with H_2O_2 is summarized, and a schematic is provided in Fig. 11. At low bicarbonate concentrations upon H_2O_2 addition, oxidative decomposition of H_2O_2 occurs at the exposed U_3O_8 surface forming a surface layer comprised of $\text{U}^{(\text{VI})}$ that provides protection against further oxidative dissolution. The decomposition of H_2O_2 proceeds *via* catalytic decomposition, and so the rate of U dissolution is low. The surface layer protects the U_3O_8 in bicarbonate concentrations up to 5 mM, and the H_2O_2 decomposition mechanism remains catalytic and U dissolution remains low. At 10 mM bicarbonate, the concentration of bicarbonate is sufficient to induce dissolution of the surface layer, and the surface layer does not fully protect the U_3O_8 which is exposed leading to oxidative decomposition of H_2O_2 and an increase in U dissolution. At higher bicarbonate concentrations, the surface layer is further dissolved, and oxidative decomposition of H_2O_2 and dissolution of U proceeds at higher rates.

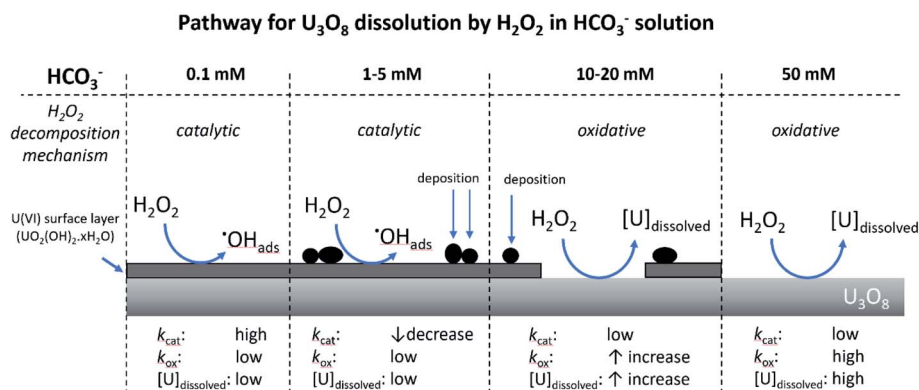


Fig. 11 The proposed pathway for U_3O_8 dissolution upon H_2O_2 addition as a function of bicarbonate concentration.

Conclusions

Based on the presented results, the effect of bicarbonate on U dissolution from U_3O_8 with H_2O_2 addition can be split into 3 sections:

(1) $[\text{NaHCO}_3] < 5 \text{ mM}$: H_2O_2 decomposition occurs *via* catalytic decomposition at the U_3O_8 surface, and the dissolution of U into solution is low.

(2) $5 \text{ mM} < [\text{NaHCO}_3] < 20 \text{ mM}$: secondary phases deposit onto the surface of the U_3O_8 upon H_2O_2 addition. The mechanism of decomposition changes from catalytic to oxidative, causing dissolution of U.

(3) $[\text{NaHCO}_3] > 20 \text{ mM}$: the decomposition mechanism of H_2O_2 is >90% oxidative, leading to significant dissolution of U.

The concentration of bicarbonate and form of uranium oxide has a large influence on U dissolution and H_2O_2 decomposition. Significant dissolution of U from U_3O_8 was observed at bicarbonate concentrations $> 5 \text{ mM}$, and the extent of U dissolution was found to be larger on U_3O_8 than for UO_2 which was attributed to the one-step oxidation of $\text{U}^{(\text{V})}$ to $\text{U}^{(\text{VI})}$ for U_3O_8 compared to the two-step oxidation for UO_2 from $\text{U}^{(\text{IV})}$ to $\text{U}^{(\text{V})}$ to $\text{U}^{(\text{VI})}$. The rate of H_2O_2 decomposition on U_3O_8 was comparable to literature data for UO_2 . However, the mechanism of H_2O_2 decomposition on U_3O_8 showed a strong dependence on the concentration of bicarbonate in solution with catalytic preferred at low bicarbonate and oxidative at high bicarbonate. The increase in catalytic activity at low bicarbonate was attributed to oxidation of the U_3O_8 surface and formation of a surface oxide.

Predicting the dissolution behaviour of spent fuel in the far future upon deep geological repository failure is a challenging task that requires significant experimental data for the development of accurate predictive models. In this work, elucidation of the mechanism of H_2O_2 decomposition on U_3O_8 and its effect on U dissolution was achieved, along with H_2O_2 decay constants as a function of simulated groundwater bicarbonate concentration. In groundwater containing high bicarbonate concentrations, significant dissolution of U from U_3O_8 is expected. This provides contributions to the development of such models for safety assessment of deep geological repositories. By demonstrating that the form of U will play a major role in the rate of U dissolution into the environment, the need for further studies regarding the effect of spent fuel composition on radionuclide dissolution into groundwater has been highlighted.

Conflicts of interest

There are no conflicts to declare.

Acknowledgements

This study was performed as part of "Project on Research and Development of Spent Fuel Direct Disposal as an Alternative Disposal Option (2020FY)" funded by the Ministry of Economy, Trade and Industry of Japan.

References

- 1 I. Casas, J. de Pablo, J. Giménez, M. E. Torrero, J. Bruno, E. Cera, R. J. Finch and R. C. Ewing, *Radiochim. Acta*, 2009, **97**, 485.
- 2 S. J. Romaniello, A. D. Herrmann and A. D. Anbar, *Chem. Geol.*, 2013, **362**, 305.
- 3 Y. Kolodny, A. Torfstein, K. Weiss-Sarusi, Y. Zakon and L. Halicz, *Chem. Geol.*, 2017, **451**, 1.
- 4 N. E. Jemison, A. E. Shiel, T. M. Johnson, C. C. Lundstrom, P. E. Long and K. H. Williams, *Environ. Sci. Technol.*, 2018, **52**, 3422.
- 5 E. Ekeröth, O. Roth and M. Jonsson, *J. Nucl. Mater.*, 2006, **355**, 38.
- 6 A. Traboulsi, J. Vandenborre, G. Blain, B. Humbert, J. Barbet and M. Fattahi, *J. Phys. Chem. C*, 2014, **118**, 1071.
- 7 R. Springell, S. Rennie, L. Costelle, J. Darnbrough, C. Stitt, E. Cocklin, C. Lucas, R. Burrows, H. Sims, D. Wermeille, J. Rawle, C. Nicklin, W. Nuttall, T. Scott and G. Lander, *Faraday Discuss.*, 2015, **180**, 301.
- 8 S. Le Caër, *Water*, 2011, **3**, 235.
- 9 S. Sunder, N. H. Miller and D. W. Shoesmith, *Corros. Sci.*, 2004, **46**, 1095.
- 10 J. S. Goldik, J. J. Noël and D. W. Shoesmith, *J. Electroanal. Chem.*, 2005, **582**, 241.
- 11 L. Wu and D. W. Shoesmith, *Electrochim. Acta*, 2014, **137**, 83.
- 12 L. Bauhn, N. Hansson, C. Ekberg, P. Fors and K. Spahiu, *J. Nucl. Mater.*, 2018, **507**, 38.
- 13 D. W. Shoesmith, *J. Nucl. Mater.*, 2000, **282**, 1.
- 14 M. M. Hossain, E. Ekeröth and M. Jonsson, *J. Nucl. Mater.*, 2006, **358**, 202.
- 15 J. De Pablo, I. Casas, J. Giménez, V. Martí and M. E. Torrero, *J. Nucl. Mater.*, 1996, **232**, 138.
- 16 S. Röllin, K. Spahiu and U. B. Eklund, *J. Nucl. Mater.*, 2001, **297**, 231.
- 17 Y. Kumagai, A. Barreiro Fidalgo and M. Jonsson, *J. Phys. Chem. C*, 2019, **123**, 9919.
- 18 G. Leinders, R. Bes, J. Pakarinen, K. Kvashnina and M. Verwerft, *Inorg. Chem.*, 2017, **56**, 6784.
- 19 K. O. Kvashnina, S. M. Butorin, P. Martin and P. Glatzel, *Phys. Rev. Lett.*, 2013, **111**, 1.
- 20 K. Sanyal, A. Khooha, G. Das, M. K. Tiwari and N. L. Misra, *Anal. Chem.*, 2017, **89**, 871.
- 21 P. Taylor, D. D. Wood, D. G. Owen and G. Park, *J. Nucl. Mater.*, 1991, **183**, 105.
- 22 A. O. Allen, C. J. Hochanadel, J. A. Ghormley and T. W. Davis, *J. Phys. Chem.*, 1952, **56**, 575.
- 23 T. K. Campbell, E. R. Gilbert, C. K. Thornhill and B. J. Wrona, *Nucl. Technol.*, 1989, **84**, 182.
- 24 K. Fukuda, Y. Watanabe, H. Murakami, Y. Amano, D. Aosai, Y. Kumamoto and T. Iwatsuki, *Hydrochemical Investigation at the Mizunami Underground Research Laboratory – Compilation of Groundwater Chemistry Data in the Mizunami Group and the Toki Granite*, Japanese Atomic Energy Agency, 2020.
- 25 B. Y. Kim, J. Y. Oh, M. H. Baik and J. I. Yun, *Nucl. Eng. Technol.*, 2010, **42**, 552.



- 26 S. S. Kim, M. H. Baik, J. W. Choi, H. S. Shin and J. I. Yun, *J. Radioanal. Nucl. Chem.*, 2010, **286**, 91.
- 27 L. F. Auque, M. J. Gimeno and J. B. Gomez, *Groundwater chemistry around a repository for spent nuclear fuel over a glacial cycle*, Swedish Nuclear Fuel and Waste Managemnt Co, 2006.
- 28 H. M. Rietveld, *J. Appl. Crystallogr.*, 1969, **2**, 65.
- 29 A. L. Patterson, *Phys. Rev.*, 1939, **56**, 978.
- 30 P. W. H. Bragg and W. L. Bragg, *Proc. R. Soc. London. Ser. A, Contain. Pap. a Math. Phys. Character*, 1913, **17**, 428.
- 31 B. O. Loopstra, *J. Inorg. Nucl. Chem.*, 1977, **39**, 1713.
- 32 S. Brunauer, P. H. Emmett and E. Teller, *J. Am. Chem. Soc.*, 1938, **60**, 309.
- 33 A. O. Allen, C. J. Hochanadel, J. A. Ghormley and T. W. Davis, *J. Phys. Chem.*, 1952, **56**, 575.
- 34 T. C. J. Overton and W. T. Rees, *Analyst*, 1950, **75**, 204.
- 35 M. M. Hossain and M. Jonsson, *J. Nucl. Mater.*, 2008, **373**, 186.
- 36 F. Clarens, J. de Pablo, I. Casas, J. Giménez and M. Rovira, *MRS Online Proc. Libr.*, 2003, **1**, 730.
- 37 D. Manara and B. Renker, *J. Nucl. Mater.*, 2003, **321**, 233.
- 38 S. Nilsson and M. Jonsson, *J. Nucl. Mater.*, 2011, **410**, 89.
- 39 T. E. Eriksen, D. W. Shoesmith and M. Jonsson, *J. Nucl. Mater.*, 2012, **420**, 409.

